ARAIM in Flight Using GPS and GLONASS: Initial Results from a Real-time Implementation

R. Eric Phelts, Juan Blanch, Yu-Hsuan Chen, Per Enge, *Stanford University*

Stuart Riley, *Trimble Navigation Limited*

ABSTRACT

Dynamic, mobile platforms offer the opportunity to analyze robustness to satellite outages due to aircraft maneuvers or other real-world situations where interruptions in continuity, in particular, can potentially be problematic. And real-time implementation serves to demonstrate the state of readiness of the algorithm to meet its intended purpose—providing high-integrity navigation for aircraft. To this end, a flight test was arranged to test ARAIM operation in flight.

For this paper, the ARAIM user algorithm was implemented using GPS and GLONASS in real-time in flight at the airport in Atlantic City, NJ. Several flight profiles were flown to inject typical aircraft dynamics into the system. The real-time data was analyzed to understand the effects of aircraft dynamics on receiver on the horizontal and vertical protection levels. It is shown that the ARAIM algorithm may be sensitive to aircraft dynamics and that adequate characterization of the multipath errors and proper mitigation of cycle slips may play a significant role in achieving expected continuity and availability.

INTRODUCTION

ARAIM proposes to use multiple constellations and satellites to enable high-integrity aviation operations worldwide with minimum ground infrastructure. Despite this objective, most of the analyses to date have relied on data from static ground reference stations. A far better platform to evaluate real-world ARAIM performance is aboard an aircraft.

Aircraft maneuvers such as banking and even turbulent flight can lead to brief satellite outages. Also, multipath reflections from the airframe may be problematic if not properly characterized. In addition, in-flight tests may turn up other unexpected issues that may need to be considered for the best ARAIM performance in the future.

A true ARAIM implementation will use a minimum of two fully-operational GNSS constellations. Each will broadcast open, coded signals on two frequencies—L1 and L5. The avionics receiver will be MOPS-certified and implementing the accepted ARAIM fault detection and exclusion algorithm. Finally, the Integrity Service Message (ISM) parameters should also be finalized and appropriate for each constellation.

For our flight test, ARAIM was implemented using the GPS and GLONASS constellations. The L1 and L2 (semi-codeless) frequencies were used for ranging and removal of the ionosphere. This served the dual-purpose of offering ease of implementation and also similarity to the prior work using a static reference station [1] [2]. Finally, a commercial (i.e., not aviation certified) receiver was used, and the ARAIM user algorithm was implemented as in [3] and [4] using the best, current ISM parameter estimates.

SETUP

The aircraft flown was a Global 5000 jet owned and operated by the William J. Hughes FAA Technical Center. The antenna used was dual-frequency (L1, L2 and G1, G2) capable and mounted atop the aircraft as indicated in Figure 1.

Figure 1. FAA Technical Center Global 5000 aircraft with GNSS antenna location indicated.

The receiver used was a Trimble BX935-INS. (See Figure 2.) The receiver was capable of tracking all the current GNSS constellations, satellites, and signals including the following:

- GPS, (L1 C/A, L1C, L2 (semi-codeless), L2C, and L5)
- WAAS (L1 C/A and L50
- GLONASS (G1 and G2)
- Galileo (E1 and E5a)
- Beidou (B1 and B2).

Note that the BX935-INS also contained an INS sensor that could be used to aid in tracking but that feature was disabled for the purposes of this test.

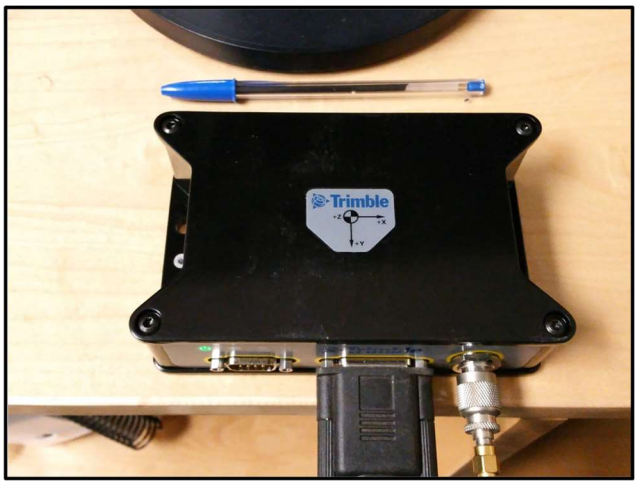

Figure 2. Trimble BX935-INS receiver

Windows Visual Studio 2010 was used to develop code that read in and parsed the BINEX data. Matlab was used to process the outputs, display the ARAIM outputs to the screen and save the results to the hard drive. (See Figure 3.)

The system was programed to process BINEX packets from the receiver at a 1-Hz rate and decode them to read the GNSS observables, ephemeris, and position data (in NMEA format). (See Figure 4.) These outputs were processed by the ARAIM algorithm.

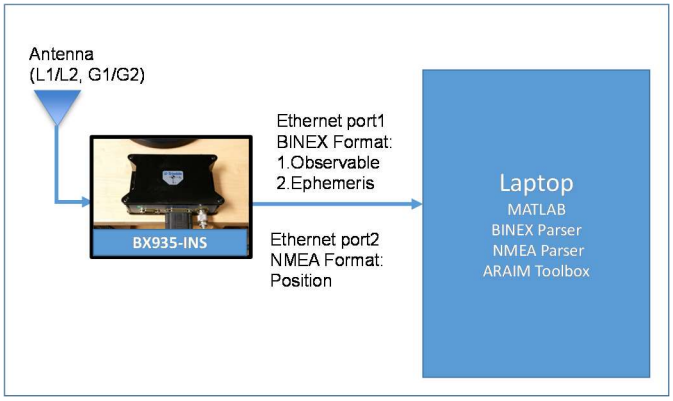

Figure 3. Hardware setup.

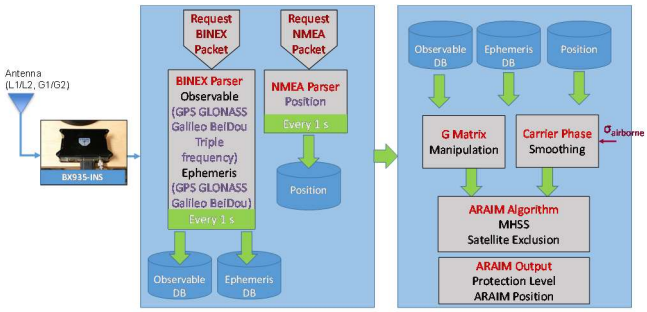

Figure 4. ARAIM software architecture.

The flight test was performed for approximately 3 hours on both August 24 and 25th of 2016 near the airport in Atlantic City, NJ.

Three flight profiles, each lasting approximately one hour, were selected to observe and evaluate the response of the ARAIM algorithm to dynamic inputs:

1) "Straight and level" flight
2) "Figure 8's"
3) Missed Approaches (3 clockwise, 3 counter-clockwise)

"Straight and Level" flight profile was selected to get a baseline for the dynamic tests. The "Figure 8's" were selected to observe the effects of banking in each direction. The missed approaches were chosen to be representative of landing, the most safety-critical phase of aviation navigation. A plan view of the flight path for day 1 of the days of testing is shown in Figure 5.

Figure 5. Plan view of all flight profiles flown for day 1

A screen-capture of the real-time system/GUI in operation is shown below in Figure 6. The upper-left corner displays the key outputs/figures of merit for the ARAIM algorithm: VPL (red), HPL (blue), effective monitor threshold or EMT (green), and $\sigma_{accuracy}$ (black). The bottom left displays the same information (in numerical values) to the screen along with the number of GPS and GLONASS SVs tracked in real-time. (The number of exclusions could be observed best on this screen.) The bottom-right shows a sky plot of all the SVs (from all constellations) being tracked by the Trimble receiver. And the top-right shows an overhead view of the flight path taken by the airplane.

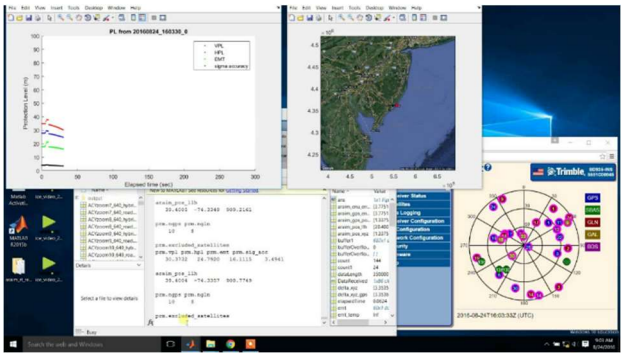

Figure 6. Screen capture of real-time GUI.

ANALYSIS

The primary parameter of interest in this test is $\sigma_{airborne}$. It is driven primarily by the characterization of the multipath component of the dual-frequency range error. This is usually assumed to be small for aircraft since 1) reflectors are generally limited to those on the airframe itself, and 2) aircraft dynamics help to "whiten" the bias making it relatively easy to mitigate through averaging, or carrier smoothing.

Three models of the predicted multipath error bounds for the carrier-smoothed, dual-frequency multipath were evaluated in this test. These models include two that were originally proposed for static platforms (e.g., WAAS reference receivers). Those two were not elevation-angle dependent and simply used two different convergence values. The third was the Working Group C (WG-C) model [5] which has an elevation angle dependence. (See Figure 7.)

It should be noted that for this test, only Model 2 yielded results that had relatively few exclusions. The others had final convergence values that proved to be too optimistic for this airframe and signal combination. This led to far too many exclusions to offer a representative analysis. Consequently, only results from Model 2 are presented in this paper.

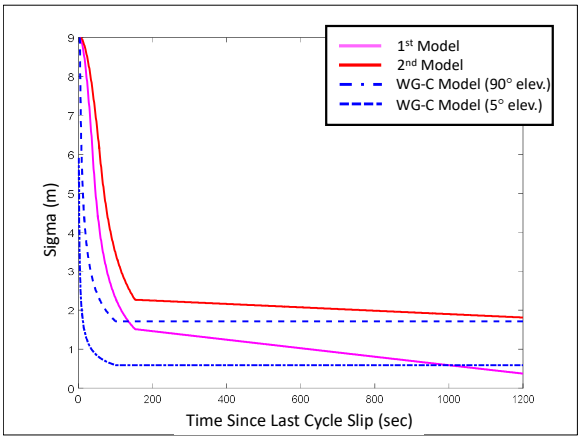

Figure 7. Three Multipath Error Models

RESULTS

Profiles of the height (i.e., altitude) vs time for both test days of the flight are shown in Figures 8 and 9. Note that for each there is a rapid ascent to the first phase of the flight. The "straight and level" phase for each test was flown manually and shows some variations, while the autopilot was used to stabilize the altitude for the "Figure 8's." For the six missed approaches, a few were "touch-and-go's," (i.e., they included a brief touchdown), however in most cases, the wheels never touched the ground.

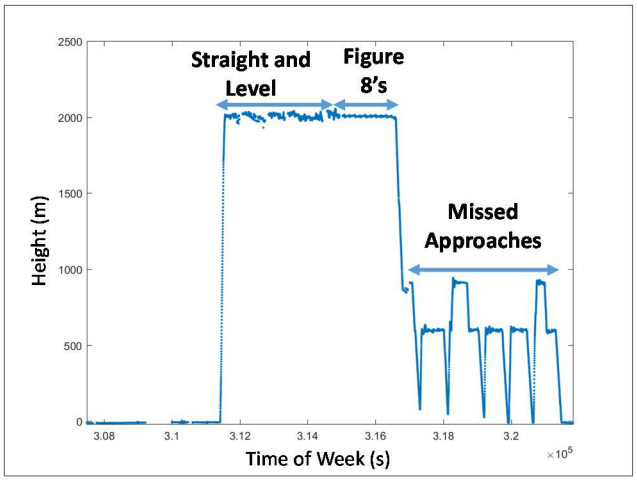

Figure 8. Altitude vs. time for flight on Day 1.

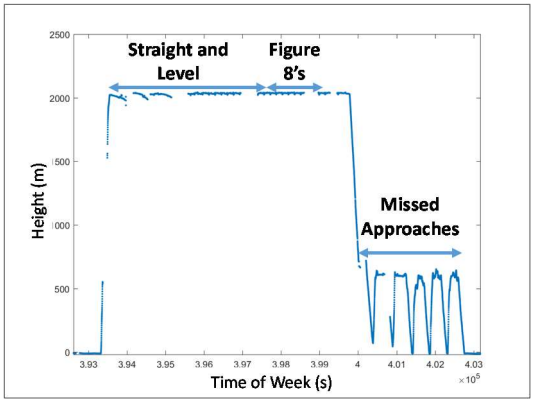

Figure 9. Altitude vs time for flight on Day 2.

Note that there are several noticeable breaks in the data on each day. These were mostly user-driven interruptions where recording was intentionally stopped to fix some issue or to update the software with new ISM or carrier smoothing/multipath model parameters. There were significantly more issues and unexpected with the hardware on Day2 two. For this reason only the ARAIM results from Day 1 and will be discussed further here.

ARAIM protection levels for the "straight and level" phase of the flight are shown in Figure 10. After re-initialization, the curves smoothly settle to nearly constant values before brief outages occur due to low-elevation SVs being lost from view. These appear to be mostly a result of multipath and perhaps some aircraft motion as well as the aircraft was mostly (but not always) completely level. This give some indication that the final settling value for the carrier-smoothing curve (Model 2) is likely still not sufficiently conservative enough to bound the multipath.

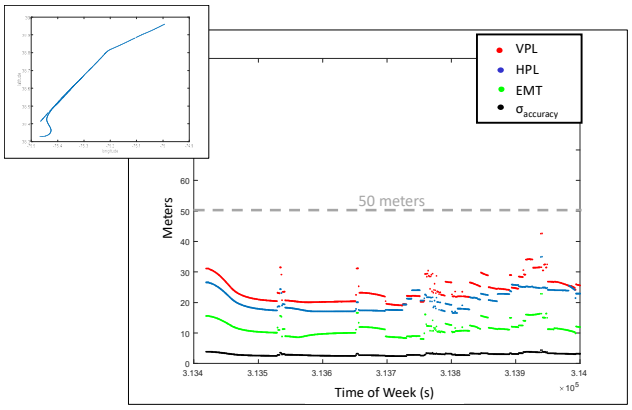

Figure 10. Protection levels for the "straight and level" phase flight on Day 1. (GPS: $P_{sat}=10^{-4}$, $P_{const}=0$; GLONASS: $P_{sat}=10^{-4}$, $P_{const}=10^{-4}$)

Figure 11 shows the figures of merit for the "Figure 8" maneuvers. In this case, we can clearly see the (periodic) effects of aircraft dynamics on the protection levels. Low-elevation satellites were regularly lost as the aircraft made successive turns, leading to momentarily increased VPLs and HPLs. There were likely also repeated carrier-smoothing resets as well as the protection levels appear to show slight sloping just after many instances of the outages.

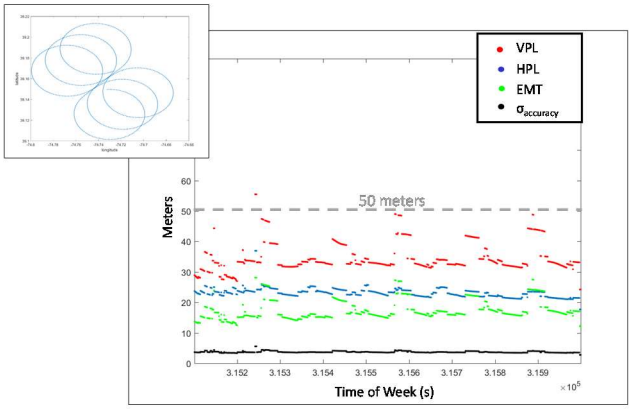

Figure 11. Protection levels for the "Figure 8's" phase of flight on Day 1. (GPS: $P_{sat}=10^{-4}$, $P_{const}=0$; GLONASS: $P_{sat}=10^{-4}$, $P_{const}=10^{-4}$)

The real-time ARAIM protection level results for a subset of the missed approaches flown on Day 1 are shown in Figure 12. As this case combines the dynamics of "straight and level" flight and with some turns, the outages are noticeably less-frequent than were observed for "Figure 8" maneuvers. The instances of level flight also are readily observable and, in fact, generally seem more stable than in the case for the "straight and level" flight. This may be due to the pilots' efforts to maintain more careful control over the aircraft attitude and dynamics while performing these more-stringent operations.

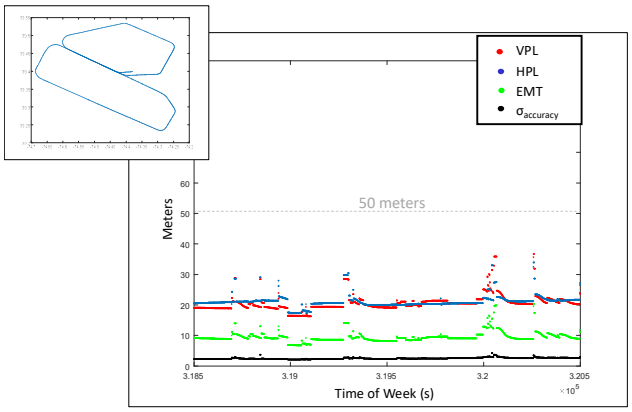

Figure 12. Protection levels for the "Figure 8's" phase of flight on Day 1. (GPS: $P_{sat}=10^{-4}$, $P_{const}=0$; GLONASS: $P_{sat}=10^{-4}$, $P_{const}=10^{-4}$)

Histograms for the HPLs and VPLs achieved for the test on Day 1 are shown in Figures 13 and 14, respectively. Most were as expected however for approximately 3% of the data, the VPLs were unusually large. This was primarily caused by three things:

1) Exclusions due to a mischaracterization of the multipath curve
2) Exclusions due to an undetected cycle slip
3) Resets of the multipath curve after a cycle slip

Semi-codeless tracking of GPS-L2 likely led to many of the observed issues with brief satellite outages, multipath, and cycle slips. Cycle slips, in particular, proved particularly challenging. Detected cycle slips caused the multipath error bound to increase thereby increasing the protection levels. The undetected cycle slips caused the error bound to grow for low-elevation satellites. The ARAIM algorithm eventually excluded them leading to increased protection levels as well.

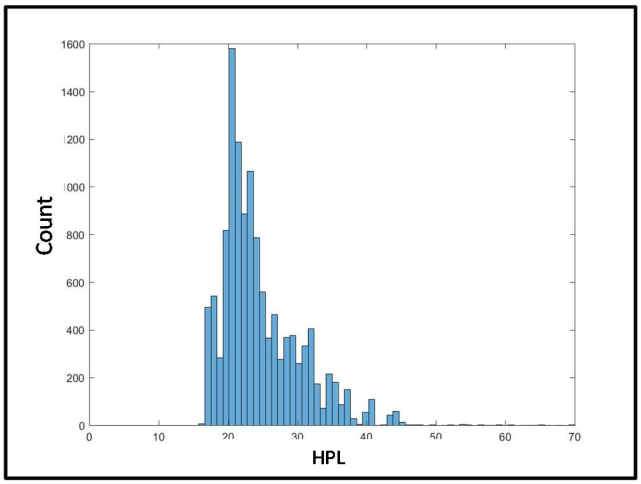

Figure 13. Histogram of the real-time HPLs for Day 1.

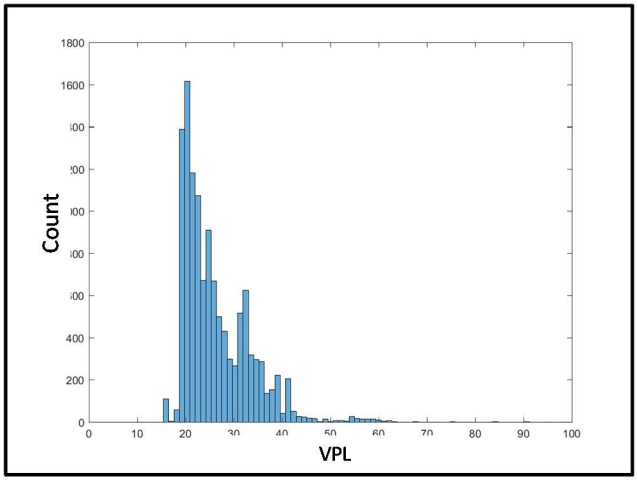

Figure 14. Histogram of the real-time VPLs for Day 1.

CONCLUSIONS

A flight test was conducted in Atlantic City to demonstrate ARAIM operation on an aircraft and operating in real-time. Since the implementation did not use true MOPS-certified receiver, GNSS satellites or signals the results are not conclusive. Despite this, several important findings can be noted.

First, it is extremely important for ARAIM to have both a conservative error bound for the multipath error and a reliable cycle slip detector. Second, aircraft maneuvers like banking could cause brief satellite outages which may affect the protection levels. Third, in-flight testing (using coded GNSS signals on L5) is needed to improve fidelity of results. Finally, in-flight testing is beneficial to help ensure predicted ARAIM performance can actually be achieved in flight.

ACKNOWLEGEMENTS

The authors gratefully acknowledge the support of the flight team at the William J. Hughes FAA Technical Center and would like to give a special thanks to Frank Lorge (for hosting and providing logistical support) and Bill Wanner.

The authors would also like to thank Trimble Navigation Limited for the use of their BX935-INS receiver and Stuart Riley for providing technical support.

REFERENCES

[1] Choi, M., Blanch, J., Walter, T., Akos, D., Enge, P., "Evaluation of Multi-constellation Advanced RAIM for Vertical Guidance Using GPS and GLONASS

Signals with Multiple Faults," *Proceedings of the 25th International Technical Meeting of The Satellite Division of the Institute of Navigation (ION GNSS 2012)*, Nashville, TN, September 2012, pp. -.

[2] Choi, M., Blanch, J., Akos, D., Heng, L., Gao, G. Walter, T., and Enge, P., "Demonstration of Multi-Constellation Advanced RAIM for Vertical Guidance using GPS and GLONASS Signals," *Proceedings of the Institute of Navigation GNSS-11*, Portland, September 2011.

[3] Blanch, J., Walter, T., Enge, P., "A Simple Satellite Exclusion Algorithm for Advanced RAIM," *Proceedings of the 2016 International Technical Meeting of The Institute of Navigation*, Monterey, California, January 2016, pp. 239-244.

[4] Blanch, J., Walter, T., Enge, P., Lee, Y., Pervan, B., Rippl, M., Spletter, A., Kropp, V., "Baseline Advanced RAIM User Algorithm and Possible Improvements," *IEEE Transactions on Aerospace and Electronic Systems*, Volume 51, No. 1, January 2015.

[5] Working Group C, ARAIM Technical Subgroup, Milestone 3 Report, February 26, 2016. Available at: http://www.gps.gov/policy/cooperation/europe/2016/working-group-c/ http://ec.europa.eu/growth/tools-databases/newsroom/cf/itemdetail.cfm?item_id=8690